BROADBAND TRAILING-EDGE NOISE PREDICTION OF A FOUR-BLADED AXIAL FAN USING A SEMI-ANALYTICAL METHOD

Gabriele GRASSO, Julien CHRISTOPHE, Christophe SCHRAM

von Karman Institute for Fluid Dynamics,
Environmental and Applied Fluid Dynamics Department,
72 chaussée de Waterloo, 1640 Rhode-Saint-Genèse, Belgium

SUMMARY

In this work, the results of the RANS simulation of the flow in a low-speed four-bladed ventilator is used to compute the wall pressure spectrum close to the trailing-edge of the blades by means of Panton and Linebarger statistical model, which uses boundary layer information. This is needed to compute the far-field noise spectrum by means of semi-analytical Amiet's theory. Both the wall pressure and the noise spectra are compared with measurements taken at CETIAT.

INTRODUCTION

The trailing-edge noise is the minimum broadband sound that a lifting surface would produce in absence of other sound mechanisms as turbulence interaction at the leading edge. This source of sound, caused by the scattering of the boundary-layer disturbances into acoustic waves, as illustrated in Figure 1, remains the only broadband noise contributor for subsonic fans operating in homogeneous stationary flows, in absence of any upstream, downstream and tip interaction. The present study aims at predicting the trailing-edge noise of a four-bladed low-speed axial fan on which an experimental campaign [6] has been conducted at CETIAT. The available experimental database is shared in a collaborative project including VKI, CETIAT and CETIM, for development and validation of numerical flow and noise prediction methods. In the present work, the flow and acoustic prediction is based on a method keeping balance between cost and accuracy that can be easily integrated in optimization chains [4, 5]. The procedure uses stationary flow computation and semi-analytical Amiet's theory [1]. The flow is first solved using OpenFOAM®, where a 3D steady RANS computation is performed using a Multiple Reference Frame method. The wall-pressure spectrum upstream the trailing-edge required in the trailing-edge noise theory is then obtained from

the wall-pressure reconstruction model of Panton and Linebarger [8] using boundary-layer information. Finally, the far-field sound pressure spectrum is computed by means of Amiet's theory. The blade is decomposed using a strip theory where every blade strip is approximated by a rectangular flat plate, the overall noise radiated from the blade being the sum of noise radiated from the different blade strips. The sound produced by the tip vortex and its possible interaction with the shroud is neglected in the present study. Comparisons with experimental available data is made for the different steps of the noise prediction procedure. The wall-pressure reconstruction spectrum is compared to measured wall-pressure spectrum at two locations on the suction side of the blade while the sound emitted from the fan is compared to overall sound measured in the CETIAT reverberant room.

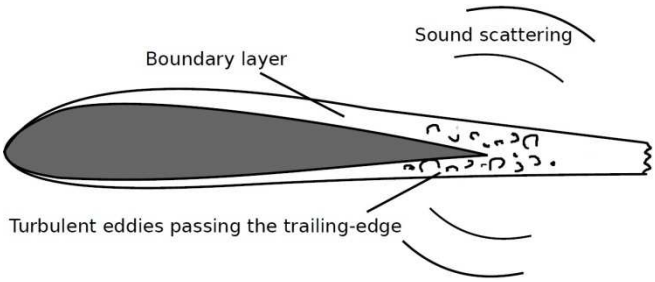

Figure 1 Trailing edge noise generation mechanism.

TRAILING EDGE NOISE COMPUTATION SEMI-ANALYTICAL METHOD

The broadband trailing-edge noise of a stationary isolated airfoil can be computed using Amiet's theory [1]. It assumes the airfoil to be infinitively thin, without camber or angle of attack, and in uniform flow conditions. The main trailing edge scattering obtained by Amiet [1] has been corrected by a leading edge back-scattering contribution which accounts for the finite chord length [11]. The radiated sound field is calculated by integrating the induced surface sources on the actual chord length, *c*, and the airfoil span, *d*, assuming convection of frozen turbulent boundary-layer eddies past the trailing edge. In the following formulas, the subscripts *1*, *2* and *3* indicate the streamwise, crosswise and spanwise directions, respectively. For large aspect ratio (*d/c*), the power spectral density of the sound pressure in the far field is obtained using:

$$S_{pp}(\mathbf{x},\omega) = \left(\frac{\omega c x_3}{2\pi c_0 S_0^2}\right)^2 \frac{d}{2} \left|\mathcal{L}\left(\frac{\omega}{U_c}\frac{\bar{k}x_2}{S_0}\right)\right|^2 \Phi_{pp}(\omega) l_y(\omega), \qquad (1)$$

where ω is the angular frequency, $\mathbf{x}$ is the position of the listener, S_0 is the distance from the source, $\mathcal{L} = \mathcal{L}_1 + \mathcal{L}_2$ is the aeroacoustic transfer function, derived analytically, with $\mathcal{L}_1$ the main contributing term from the trailing edge and $\mathcal{L}_2$ the back-scattering term from the leading edge [11]. $\Phi_{pp}(\omega)$ is the wall-pressure spectrum upstream the trailing edge while $l_y(\omega)$ is the corresponding span-wise correlation length. In the computations, $l_y(\omega)$ has been modeled by using Corcos' formulation,

$$l_y(\omega) = \frac{\omega/(b\,U_c)}{k_y^2 + (\omega/(b\,U_c))^2}$$

where $b = 1.49$ and U_c is the convection velocity. Equation (1) derives from the assumption of large-span airfoils, implying that for each listener position there will be only one radiating span-wise aerodynamic wave number. It is interesting to notice that, according to previous tests, in a direct strip method such as the one adopted in this work, the general finite-span formula is inaccurate [2].

Using the model developed by Panton and Linebarger [8], Remmler *et al.* [9] implemented the following expression for the wall-pressure spectrum

$$\Phi_{pp}(\omega) \;=\; 8\,\rho_0^2 \iiint_0^\infty \frac{k_1(\omega)^2}{k(\omega)^2}\,\exp^{-k(\omega)(y+\hat{y})}\;S_{22}(y,\hat{y},\omega)\,\frac{\partial U_1}{\partial y}\,\frac{\partial U_1}{\partial \hat{y}}\,dy\,d\hat{y}dk_3 \qquad (2)$$

where ρ_0 is the reference density and y is the wall normal distance. The energy spectrum of the vertical velocity fluctuations, S_{22}, is expressed as:

$$S_{22}(y,\hat{y},\omega) \;=\; \frac{\bar{u_2'}(y)\,\bar{u_2'}(\hat{y})}{\pi^2}\,\Lambda^2 \iint_0^\infty R_{22}\cos(\alpha\,k_1(\omega)\,r_1)\;\cos(\alpha\,k_3\,r_3)\,dr_1\,dr_3 \qquad (3)$$

The model therefore uses the streamwise mean velocity profile $U_1(y)$ and the crosswise velocity fluctuation profile $u_2'(y)$. Both velocities and the turbulence integral length scale, Λ, are calculated from the RANS result. The velocity correlation function, R_{22}, and the scale anisotropy factor, α, need to be modeled. No quadratures are used to calculate the quintuple integral in Eq. (2) as they would require prohibitive memory. The integration is performed with a Monte Carlo method using importance sampling to enhance convergence, clustering the points where the integral is evaluated in the regions of interest with the use of a probability density function. More details on this model can be found in Remmler *et al.* [9].

In case of rotation, the far-field noise PSD of a low solidity fan with *B* independent blades is given by an integration over all possible azimuthal positions, ψ, of the single airfoil formulation [3]:

$$S_{pp}(\mathbf{X},\omega) = \frac{B}{2\pi}\int_0^{2\pi} \frac{\omega_e(\Psi)}{\omega} S_{pp}^{\Psi}(\mathbf{x},\omega_e)d\Psi \qquad (4)$$

where $\boldsymbol{X}$ is the position of the listener in the absolute frame of reference and $\mathbf{x}$ is its position in the rotating frame attached to the blade strip.
The factor $\omega_e(\Psi)/\omega$ accounts for Doppler effects due to the rotation, being ω_e the emitted frequency and ω the observed frequency. In order to take into account the variation of the flow along the airfoil span, a strip theory is used, splitting the blade in a given number of segments. The total radiated sound is then the summation of sound emitted by each airfoil strip. In the present case, the blade is split in 5 strips.

TEST CASE: FOUR-BLADED VENTILATOR

Experimental set-up

The ventilator, visible in Figure 2, has 0.8 m diameter and hub ratio of 0.34. It has four equally spaced blades, two being equipped with unsteady pressure sensors in order to measure the data required for the trailing-edge noise prediction model, namely the wall pressure spectrum and the spanwise correlation length spectrum. The chord at tip is 0.135 m and the blade's maximum thickness is 4 mm, while the mean tip gap is 5 mm. The shroud trailing-edge is aligned with that of the blade when the stagger angle of the blade is set to 30°. The shroud is mounted on the wall between the two rooms. A rotating microphone performs the acoustic measurements in the reverberant chamber, while three fixed microphones are placed downstream of the ventilator, allowing to make a spatial average of the acoustic data [6].

CFD evaluation of the test case

A three-dimensional steady RANS computation of the flow in the experimental set-up has been performed by means of OpenFOAM® 2.3. The flow has been solved in the maximum flow rate

condition (4.29 $m^3 \cdot s^{-1}$) for 600 RPM rotational speed. Given the low Mach number of the present case, the incompressible solver simpleFoam solver has been selected. Figure 3 depicts the computational domain with the related boundary conditions.

The domain is divided in three main regions: a stationary region upstream of the ventilator, containing the inlet boundary, a moving reference frame (MRF) region surrounding the ventilator and, finally, another stationary region downstream of the ventilator, containing the outlet boundary. Non-conformal interfaces (defined as cyclicAMI in OpenFOAM®) separate the MRF from the stationary regions. The same kind of interface has been applied to the lateral periodic patches which allow to simulate only one quarter of the ventilator geometry.

In order to ease the convergence, the flow rate has been imposed at the inlet, while a fixed pressure has been imposed at the outlet. The selected turbulence model is k-ω SST [7]. The results presented here are related to a boundary conditions of 5% turbulence intensity and 0.01 m turbulent length scale imposed at the inlet. Nevertheless, computations have been run at 1% inlet turbulence intensity, showing minor discrepancies in terms of predicted wall pressure spectrum with respect to the case with 5% turbulence intensity. Finally, the stationary walls upstream and downstream of the ventilator, the hub, the blade and the shroud have been defined as no-slip surfaces.

Figure 2 Experimental set-up.
The unsteady pressure sensor are visible on the upper and lower blade.

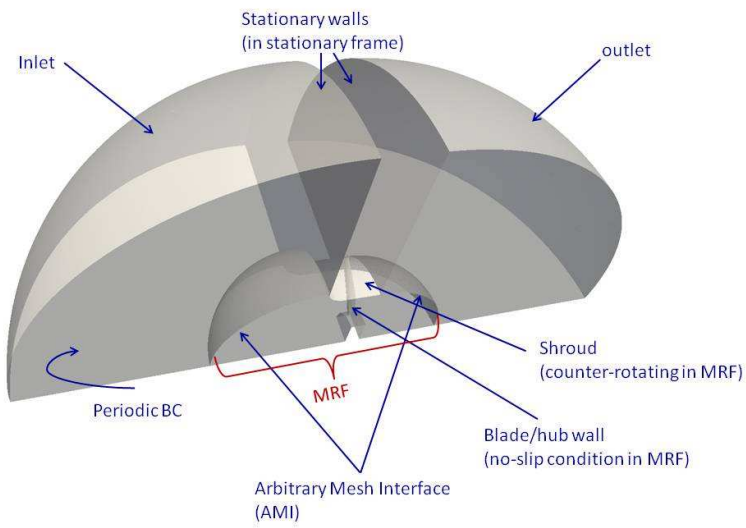

Figure 3 Computational domain with the related boundary conditions.

The computational grid has been produced using the open source tool snappyHexMesh, which can generate three-dimensional meshes containing hexahedra and split-hexahedra automatically from triangulated surface geometries. A boundary layer mesh has been applied to the blade/hub wall and to the shroud. A grid independence study has been performed by producing four different meshes of 1.5, 3.4, 7.2 and 13.9 millions of cells, respectively. Figure 4 shows a good correspondence between the pressure coefficient computed at mid-span by using the two most refined meshes. Furthermore, as can be seen in Figure 5, the grid of 7.2 M cells is refined enough to have y+ < 1 at the first cell on the blade surface. For these reasons, the mesh consisting of 7.2 M of nodes seems to be a reasonable compromise between numerical accuracy and computational time

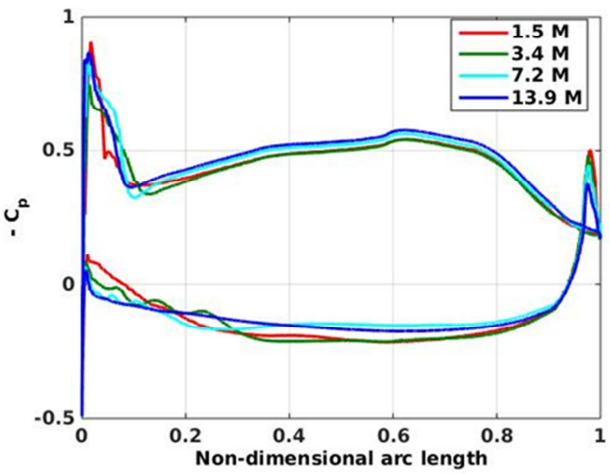

Figure 4 Pressure coefficient at mid-span for the different meshes.

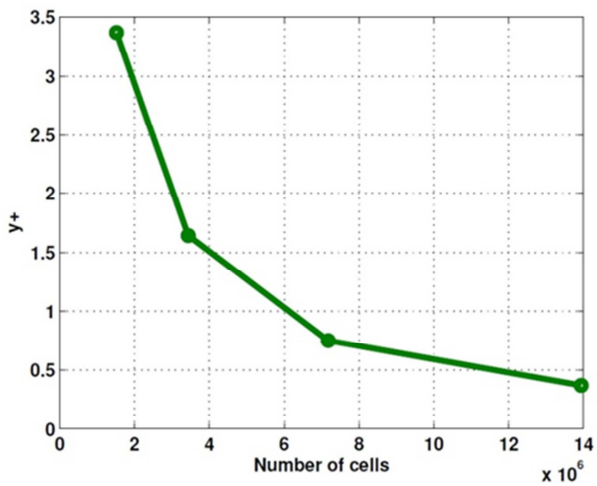

Figure 5 Evolution of the average y+ on the blade surface with the number of mesh cells.

Figure 6 represents the relative velocity field close to the hub (6a), at mid-span (6b) and in the vicinity of the tip (6c). The flow field is affected by the small axial extent of the hub, as can be seen at the lower radius, resulting in a huge separation zone on the pressure side. Since the maximum flow rate does not correspond to the maximum efficiency point, the flow is still separated on the pressure side at mid-span, but it re-attaches towards the tip, where the only detached zone is found

on the suction side close to the trailing-edge. For this reason, it may be considered to study this geometry in the best efficiency point, which is more representative of the technology under investigation.

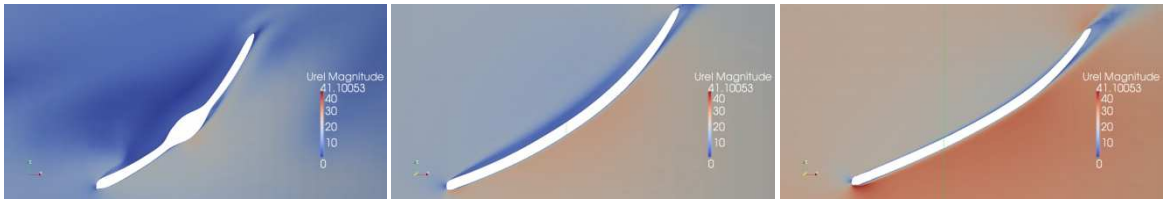

(a) *(b)* *(c)*

Figure 6 Relative velocity magnitude at different iso-radius planes.

As described in the previous Section, the wall pressure spectrum prediction model requires three inputs from the CFD computation: the streamwise mean velocity profile $U_1(y)$, the crosswise velocity fluctuation profile $u_2'(y)$ and the turbulence integral length scale, Λ. These quantities are extracted, for each blade strip, along a line normal to the blade surface starting from a point close to the trailing edge [10]. This procedure is fully automated and it is executed by a Matlab® script.

Computation of the trailing-edge wall pressure spectrum and of the ensuing noise

Figure 7 shows the comparison of the wall pressure spectrum measured close to the trailing edge and the one computed by means of Panton and Linebarger's model (Equations 2 and 3). The boundary layer data, that are the necessary input to the model, have been extracted at the same location as the pressure sensors on the blade surface. The correspondence between the two curves is better in the range from 10^3 to 10^4 Hz, while the gap increases at lower frequencies. In this respect, it is necessary to remind that the accuracy of the unsteady pressure sensors decreases below 300 Hz.

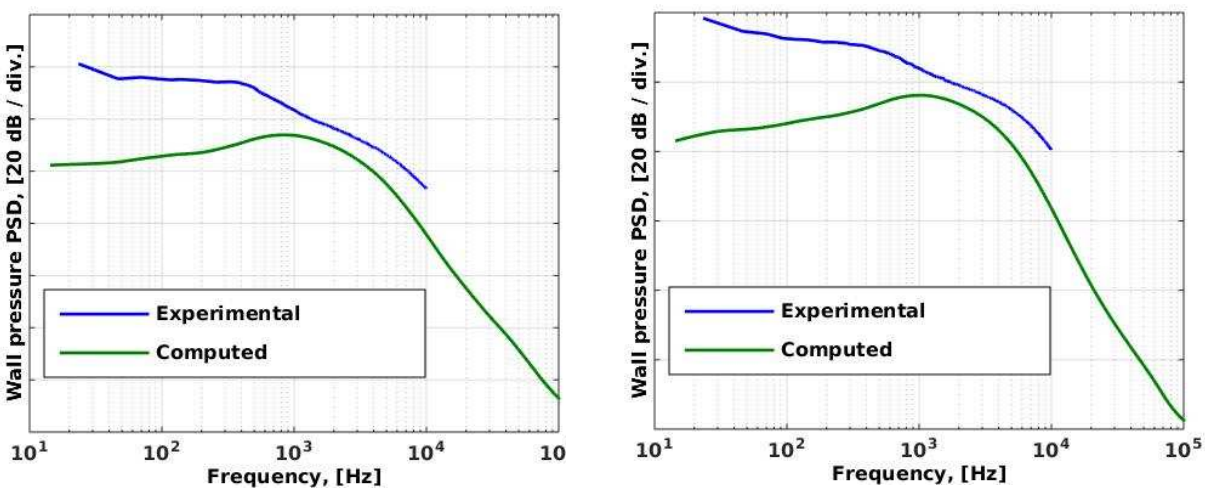

(a) R = 0.270 m *(b) R = 0.357 m*

Figure 7 Comparison of the trailing-edge wall pressure spectra measured and computed with Panton and Linebarger's model.

Having computed the wall pressure spectra at five equally spaced radial locations of the blade suction side, it is possible to compute the broadband noise radiated in far-field according to Amiet's theory (Equations 1 and 5) by summation of the noise emitted by the different strips. As can be observed in Figure 8, there is a strong discrepancy between the measured and the computed noise above 2 kHz. The reasons of this phenomenon still need to be inquired.

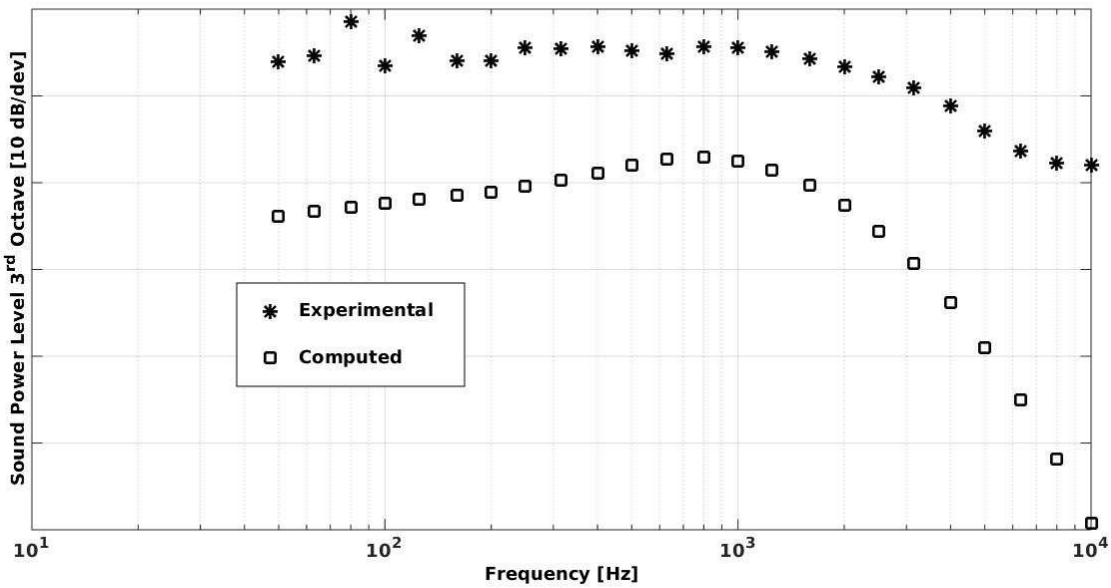

Figure 8 Comparison between the measured and the reconstructed sound power level in third octave bands.

CONCLUSIONS AND FUTURE WORK

In this paper, a procedure for the computation of the trailing-edge wall pressure spectrum in a low-speed fan has been presented and applied to a test case where an experimental database is available for comparison. This procedure is based on the extraction from steady RANS simulations of boundary layer data close to the trailing-edge of the blade, which are the input to Panton and Linebarger's model for the computation of the wall pressure spectrum. The flow data were generated with OpenFOAM® and the independence from the grid size has been assessed. Finally, a comparison between the computed wall pressure and sound spectra with the corresponding experimental data has been made. In both cases, the accuracy of the algorithm can be improved by investigating the reasons of the discrepancies in certain ranges of frequencies. The next objective of this research will be to run a scale resolved simulation of the ventilator in order to solve the unsteady pressure field and compute the wall pressure spectrum without need of statistical modeling. The comparison with the results obtained from scale resolved simulation will help in the further assessment of the capabilities of our RANS based noise prediction model.

ACKNOWLEDGMENTS

The Authors gratefully acknowledge the support of the EC under the project FlowAirS (Grant Agreement n° 289352) and Alain Guédel and Mirela Robitu of CETIAT (Lyon, France), for providing the geometry of the four bladed ventilator with the measured wall pressure and noise spectra.

BIBLIOGRAPHY

[1] R. K. AMIET, *Noise due to Turbulent Flow past a Trailing Edge*, Journal of Sound and Vibration, 47 (**1976**), pp. 387–393.

[2] J. CHRISTOPHE AND J. ANTHOINE, *Amietâ€™s theory in spanwise-varying flow conditions*, AIAA Journal, 47 (**2009**).

[3] J. CHRISTOPHE, L. SANJOSE, AND S. MOREAU, *Uncertainty quantification of low-speed axial fan self noise*, in 14th International Symposium on Transport Phenomena and Dynamics of Rotating Machinery, (**2012)**.

[4] G. GRASSO, J. CHRISTOPHE, C. SCHRAM, AND T. VERSTRAETE, *Aerodynamic, aeroacoustic and structural optimization of a contra-rotating fan*, in 15th International Symposium on Transport Phenomena and Dynamics of Rotating Machinery, (**2014)**.

[5] G. GRASSO, J. CHRISTOPHE, C. SCHRAM, AND T. VERSTRAETE, *Influence of the noise prediction model on the aeroacoustic optimization of a contra-rotating fan*, in 20th AIAA/CEAS Aeroacoustics Conference, (**2014)**.

[6] A. GUÉDEL, M. ROBITU, AND C. DHAUSSY, *Prévision du bruit de bord de fuite d'un ventilateur hélicoïde à quatre pales*, tech. report, CETIAT (**2010)**.

[7] F. R. MENTER, *Two-equation eddy-viscosity turbulence models for engineering applications*, AIAA Journal, 32 (**1994**), pp. 1598–1605.

[8] R. L. PANTON AND J. H. LINEBARGER, *Wall Pressure Spectra Calculations for Equilibrium Boundary Layers*, J. Fluid Mech., 65 (**1974**), pp. 261–287.

[9] S. REMMLER, J. CHRISTOPHE, J. ANTHOINE, AND S. MOREAU, *Computation of Wall-Pressure Spectra from Steady Flow Data for Noise Prediction*, AIAA Journal, 48 (**2010**), pp. 1997–2007.

[10] S. REMMLER, J. CHRISTOPHE, J. ANTHOINE, AND S. MOREAU, *Computation of wall-pressure spectra from steady flow data for noise prediction*, AIAA Journal, 48 (**2010**), pp. 1997–2007.

[11] M. ROGER AND S. MOREAU, *Back-Scattering Correction and Further Extensions of Amiet's Trailing-Edge Noise Model. Part 1: Theory*, Journal of Sound and Vibration, 286 (**2005**), pp. 477–506.